JACS Au
AN OPEN ACCESS JOURNAL OF THE AMERICAN CHEMICAL SOCIETY

pubs.acs.org/jacsau
Letter

Atroposelective Synthesis of Aldehydes via Alcohol Dehydrogenase-Catalyzed Stereodivergent Desymmetrization

Published as part of JACS Au virtual special issue "Biocatalysis in Asia and Pacific".

Mengjing Ye,[#] Congcong Li,[#] Dongguang Xiao, Ge Qu, Bo Yuan,* and Zhoutong Sun*

Cite This: *JACS Au* 2024, 4, 411−418

Read Online

ACCESS | Metrics & More | Article Recommendations | Supporting Information

ABSTRACT: Axially chiral aldehydes have emerged recently as a unique class of motifs for drug design. However, few biocatalytic strategies have been reported to construct structurally diverse atropisomeric aldehydes. Herein, we describe the characterization of alcohol dehydrogenases to catalyze atroposelective desymmetrization of the biaryl dialdehydes. Investigations into the interactions between the substrate and key residues of the enzymes revealed the distinct origin of atroposelectivity. A panel of 13 atropisomeric monoaldehydes was synthesized with moderate to high enantioselectivity (up to >99% ee) and yields (up to 99%). Further derivatization allows enhancement of the diversity and application potential of the atropisomeric compounds. This study effectively expands the scope of enzymatic synthesis of atropisomeric aldehydes and provides insights into the binding modes and recognition mechanisms of such molecules.

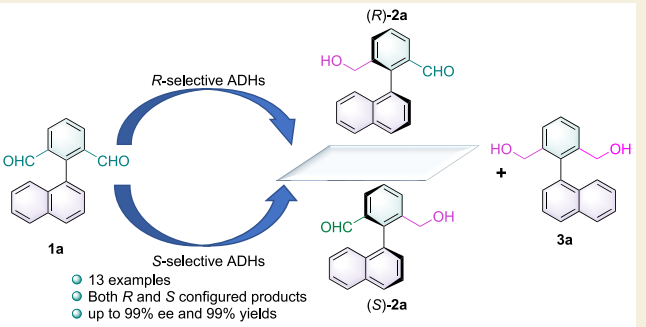

KEYWORDS: *atropisomers, axially chiral compounds, alcohol dehydrogenases, desymmetrization, biaryl aldehydes*

INTRODUCTION

Atropisomerism refers to stereoisomerism caused by restricted bond rotation and was discovered by Christie and Kenner in 1922.[1] It frequently constitutes vital structural elements for natural products,[2−5] functional materials,[6,7] molecular machines,[8] and bioactive molecules.[9−11] Various strategies have been developed for the construction of the stereogenic axis or asymmetric induction after formation of the atropisomeric bond, including desymmetrization, kinetic resolution (KR), and dynamic kinetic resolution (DKR).[12−19] Various synthetic methodologies, such as organocatalysis[20,21] utilizing *N*-heterocyclic carbene (NHC),[22−27] chiral phosphoric acid (CPA),[28−33] chiral secondary amine,[34] thiourea,[35,36] and peptide[37] catalysts, have been reported in the past decade. Metal catalysis has also been applied in the atroposelective synthesis utilizing Cu,[38] Pd,[39−41] Ir,[42] and Rh[43] catalysts. Very recently, Yang and co-workers reported the CPA-catalyzed desymmetrization of diaryl ether amines with azodicarboxylates, which afforded diaryl ethers in up to 99% yields and >99% ee (Scheme 1a).[28] Other desymmetrization strategies were reported by Zhu et al., who employed the imidodiphosphorimidate (IDPi)-catalyzed silylation of biaryl diols to enable the atroposelective kinetic resolution with up to 77% yields and 98.5:1.5 er (Scheme 1b).[44] In addition, Wu et al. reported the NHC-catalyzed desymmetrization followed by kinetic resolution of biaryl dialdehydes to afford 47 value-added, structurally diverse aldehydes in up to 97% yields and >99% ee (Scheme 1c).[45] However, requirements for directing groups and additional removal steps; difficulties in the synthesis of the complex chiral ligands, auxiliaries, or catalysts; and stoichiometric addition of selected catalysts or reagents are often encountered in chemical synthetic methods. Conversely, biocatalytic asymmetric synthesis of axially chiral compounds may offer distinct advantages, such as environmental benignity, mild conditions, and superior selectivity. Currently, only a handful of examples have been reported so far to synthesize biaryls in high atroposelectivity during the past decade utilizing biocatalysis.[46,47] Enzymatic atroposelective coupling reactions by laccases,[48] copper-dependent oxidase,[49] and cytochrome P450 enzymes[50−52] have been previously explored, albeit with very limited substrate scope and atroposelectivity. Recently, flavin-dependent halogenases (FDHs) have enabled highly stereoselective DKR of 3-aryl-4(3*H*)-quinazolinones; nevertheless, the substrate loadings were limited, thus preventing further application utility. Vanadium chloroperoxidase from

Received: December 20, 2023
Revised: January 19, 2024
Accepted: January 22, 2024
Published: February 8, 2024

https://doi.org/10.1021/jacsau.3c00814
JACS Au 2024, 4, 411−418

Scheme 1. Representative Atroposelective Desymmetrizations

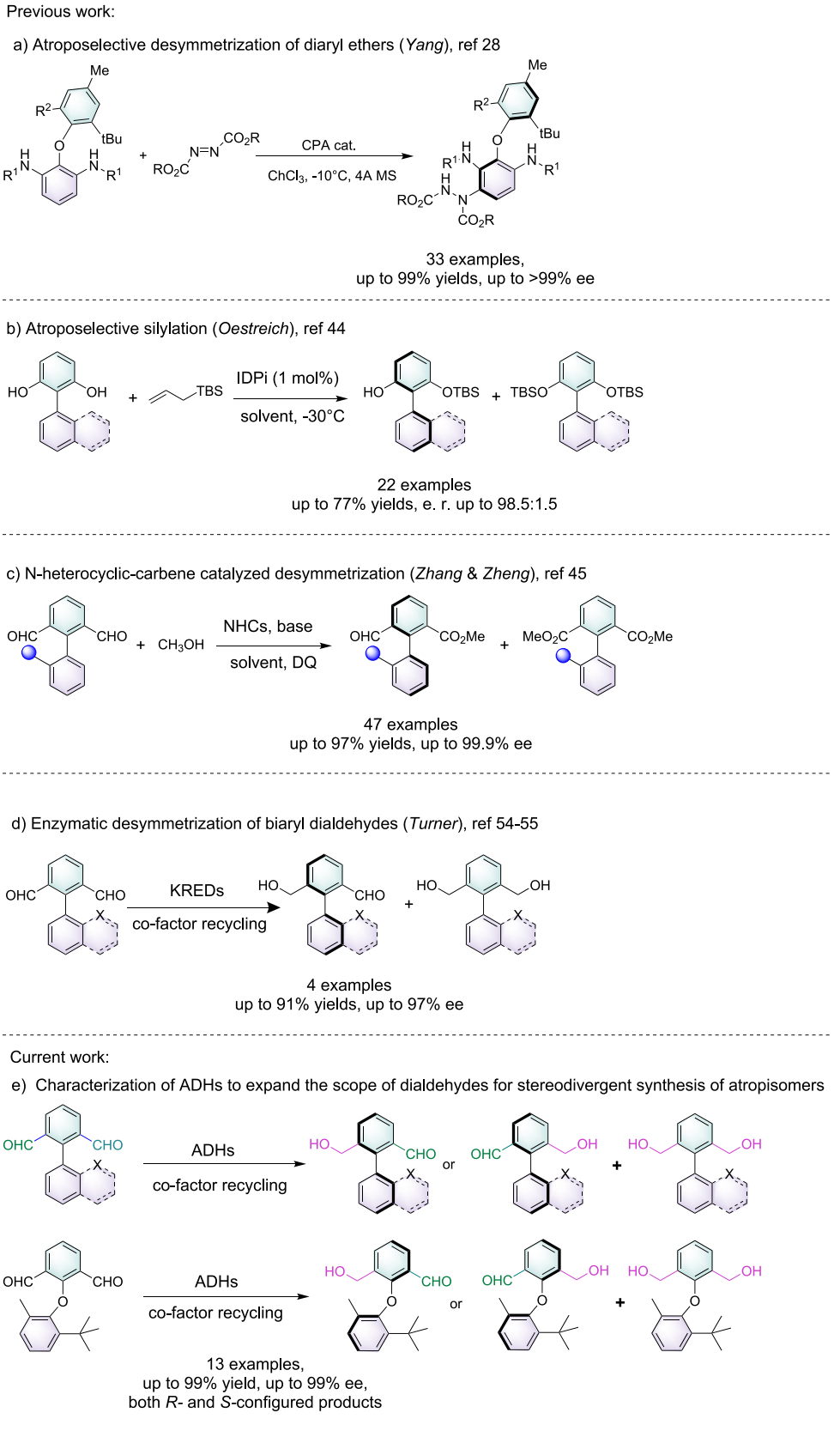

Curvularia inaequalis (*Ci*VCPO) can catalyze the tribromination of biaryls to transform the freely rotating biaryl axis to sterically hindered bond, but only in racemic forms.[53] We and others have established that ketoreductases (KREDs) or

https://doi.org/10.1021/jacsau.3c00814
JACS Au 2024, 4, 411−418

Table 1. Screening of ADHs Utilizing 1a as the Model Substrate[a]

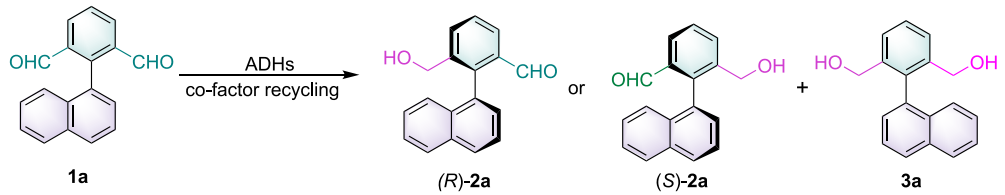

1a (*R*)-2a (*S*)-2a 3a

entry	enzyme	sources	types	2a [%]	3a [%]	ee [%]	configuration of 2a
1	ADH-R1	*Burkholderia gladioli*	SDR	94.3 ± 3.1	3.0 ± 0.8	80.4 ± 0.8	*S*
2	ADH-R2	*Ralstonia sp.*	SDR	92.4 ± 2.5	1.9 ± 0.9	99.9 ± 0.1	*S*
3	ADH-R3	*Lactobacillus kefiri*	SDR	47.7 ± 0.3	1.6 ± 0.3	70.1 ± 0.7	*S*
4	ADH-R4	*Oenococcus alcoholitolerans*	SDR	87.5 ± 0.7	11.4 ± 1.8	99.4 ± 0.2	*S*
5	ADH-R5	*Zymomonas mobilis*	MDR	87.9 ± 1.8	2.9 ± 0.4	88.3 ± 0.0	*R*
6	ADH-R6	*Parageobacillus thermoglucosidasius*	MDR	90.6 ± 1.8	2.6 ± 0.4	92.5 ± 1.5	*R*
7	ADH-R7	*Thermus thermophilus*	SDR	95.4 ± 0.3	3.7 ± 0.3	99.9 ± 0.1	*R*
8	ADH-R8	*Rhodopseudomonas palustris*	MDR	93.5 ± 1.4	2.9 ± 0.6	95.5 ± 5.4	*R*
9	ADH-R9	*Rhizobium etli*	MDR	96.7 ± 1.2	2.9 ± 1.0	99.4 ± 0.1	*R*
10	ADH-R10	*Pseudomonas meliae*	MDR	95.5 ± 0.9	4.3 ± 0.9	99.9 ± 0.1	*R*

[a]Reaction conditions: **1a** (10 mM), $NADP^+$ (1 mM), glucose (20 mM), glutamate dehydrogenase (GDH) (2.5 mg mL^{-1}), ADHs (0.1 g mL^{-1} of whole cell with 6 units mL^{-1} of DNaseI and 1 mg mL^{-1} of lysozyme), DMSO (5% v/v) in NaPi buffer (pH 7.4, 50 mM), at 30 °C, 800 rpm. Total volume: 1 mL.

alcohol dehydrogenases (ADHs) can be utilized in the desymmetrization, KR, and DKR of biaryl dialdehydes or diaryl ethers (Scheme 1d).[54−56] However, the scope was limited to less than five substrates, the mechanisms of enzymatic atroposelective recognition for biaryls or diaryl ethers were not investigated, and only a limited number of commercial KREDs have been utilized. In this endeavor, we demonstrate that screening against a large panel of structurally diverse ADHs enables the synthesis of both (*R*)- and (*S*)-configured atropisomeric biaryls (Scheme 1e), and the differences in the interactions between the substrates and the enzymes have led to the stereodivergent desymmetrization of the biaryl and diaryl ether dialdehydes.

RESULTS AND DISCUSSION

To first identify highly active and selective ADHs toward the biaryl substrates, we employed **1a** as the model substrate to screen a panel of 92 ADHs (phylogenetic analysis of the ADHs is shown in Figure S1) from a variety of sources (full panel results are shown in Tables S3 and S4). To our delight, a number of wild-type ADHs displayed high activity toward **1a**, which led to either (*R*)- or (*S*)-**2a**. The 10 best-performing ADHs that exhibited the highest activity and selectivity were selected (Table 1). The turnover number (TON, $[product]_{final} \times [catalysts]^{-1}$) of ADH-R9 was up to 481 (the enzyme content was estimated as shown in Figure S2). ADH-R2 and ADH-R4 afforded the (*S*)-**2a** in ee > 99%, whereas ADH-R7, ADH-R9, and ADH-R10 afforded (*R*)-**2a** with ee > 99%. The yields of **2a** were also high (>87%). A majority of short-chain dehydrogenases (SDRs) (except ADH-R7) displayed clear preference toward (*S*)-**2a**, and all medium-chain dehydrogenases (MDRs) displayed preference toward (*R*)-**2a**.

Subsequently, the substrate concentrations and the compositions of the cosolvent DMSO were optimized (Figures S4 and S5). Ten mM **1a** in sodium phosphate buffer (NaPi buffer) with 5% DMSO was selected as the optimal reaction conditions. The temperature and pH of the reactions were employed with reference to previous reports.[55] Time-course profiles of the desymmetrization of **1a** by the 10 best-performing enzymes were investigated to examine the formation of **2a** (Figures S6−S15). The over-reduced product **3a** can also be observed in <5% conversions when catalyzed by a majority of the ADHs except ADH-R4 (11.4%, Table 1, entry 4). The ee for **2a** reached a maximum in 3−6 h in all cases, but the yields of **2a** exhibited different time-course profiles for various enzymes. For example, **2a** was consumed rapidly after 3 h when the reaction was catalyzed by ADH-R1 and R2 compared with no consumption after reaching the maximum yield with ADH-R7-R9. We also performed the kinetic resolution of *rac*-**2a** employing selected ADHs, and indeed, the catalytic activities varied among different enzymes. As shown in Table S5, while ADH-R3, ADH-R5-6, and ADH-R8 are inactive toward *rac*-**2a**, the rest of enzymes are able to catalyze the kinetic resolution of **2a** with moderate conversions. ADH-R2 exhibited the highest activity for kinetic resolution of **2a**, and therefore, as shown in Figure S7, the composition of **2a** rapidly declined after 3 h. The ee of **2a** did not decrease since the desymmetrization formed (*S*)-**2a**, and the kinetic resolution consumed (*R*)-**2a**, and *vice versa*. The absolute configuration of the substrates was confirmed by comparison with reported analytical methodologies,[55] and the rotation barriers of the monoaldehydes have also been reported previously.[54]

Having established the optimal reaction conditions, the generality of the ADH-catalyzed desymmetrization of biaryl dialdehydes was explored. First, the scope of the biaryl framework of the dialdehydes was examined (Scheme 2). A variety of substrates **1b−m** were synthesized and characterized. The racemic standards for **2a−m** were established by reducing the dialdehydes by boronic hydride reagents (Figures S16−S47). The electronic effects on the naphthalene ring of the dialdehydes were investigated by varying the functional motifs. Substrates bearing electron-withdrawing (F) and electron-donating (Me, OMe) substituents are well tolerated to afford desired products **2b−2d** in good yields (up to 98%) and ee (up to 99% for *R*-configuration and up to 98% for *S*-configuration). Excellent ee could also be obtained for the phenanthrene-substituted product (*S*)-**2f**. Substrates bearing

https://doi.org/10.1021/jacsau.3c00814
JACS Au 2024, 4, 411−418

Scheme 2. Substrate Scope for the ADH-Catalyzed Desymmetrization of Prochiral Dialdehydes[a]

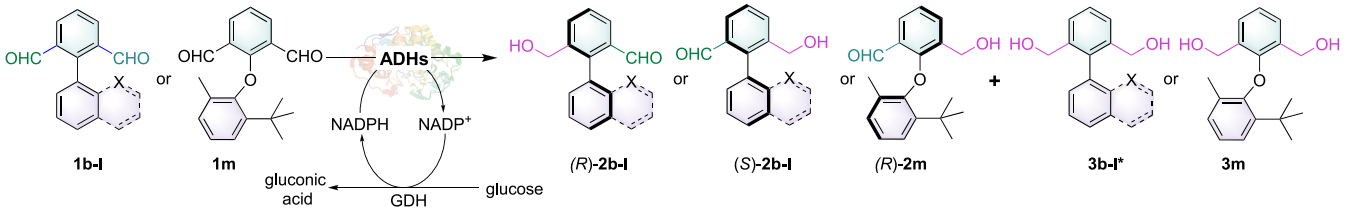

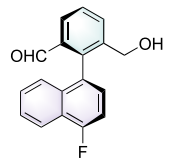

(S)-**2b**

ADH-R1 : 95%, 98% ee
ADH-R2 : 92%, > 99% ee
ADH-R4 : 97%, > 99% ee

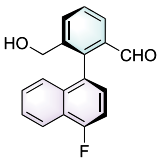

(R)-**2b**

ADH-R7 : 51% , 93% ee
ADH-R9 : 84% , 95% ee
ADH-R10 : 65%, 96% ee

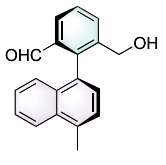

(S)-**2c**

ADH-R1 : 84%, 24% ee
ADH-R2 : 87%, > 99% ee
ADH-R4 : 96%, > 99% ee

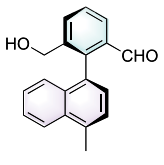

(R)-**2c**

ADH-R7 : 85%, 88% ee
ADH-R9 : 62%, 82% ee
ADH-R10 : 51%, 78% ee

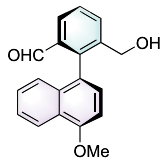

(S)-**2d**

ADH-R2 : 75%, > 99% ee
ADH-R4 : 42%, > 99% ee

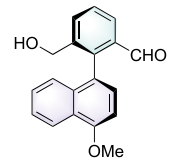

(R)-**2d**

ADH-R1 : 65%, 48% ee
ADH-R7 : 19%, 2% ee
ADH-R9 : 23%, 13% ee

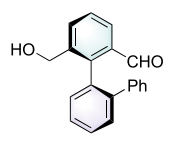

(S)-**2e**

ADH-R2 : 43%, > 99% ee

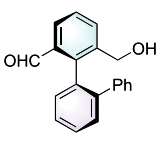

(R)-**2e**

ADH-R4 : 14%, > 99% ee

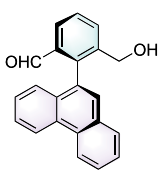

(S)-**2f**

ADH-R2 : 9%, > 99% ee
ADH-R4 : 24%, > 99% ee

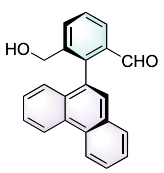

(R)-**2f**

ADH-R1 : 28%, 82% ee

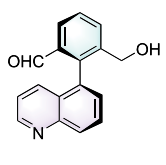

(S)-**2g**

ADH-R1 : > 99%, > 99% ee
ADH-R2 : > 99%, > 99% ee
ADH-R4 : > 99%, > 99% ee

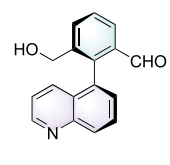

(R)-**2g**

ADH-R7 : 58%, 18% ee
ADH-R9 : 75%, 25% ee
ADH-R10 : 53%, 14% ee

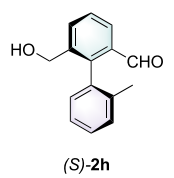

(S)-**2h**

ADH-R1 : 91%, 48% ee
ADH-R2 : 58%, 91% ee
ADH-R4 : > 99%, > 99% ee

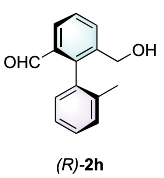

(R)-**2h**

ADH-R7 : 73%, 73% ee
ADH-R9 : 88%, 88% ee
ADH-R10 : 82%, 76% ee

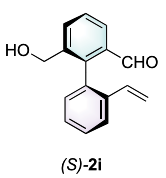

(S)-**2i**

ADH-R1 : > 99%, > 99% ee
ADH-R2 : > 99%, > 99% ee
ADH-R4 : 97%, > 99% ee

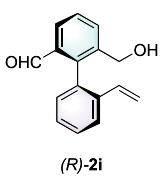

(R)-**2i**

ADH-R7 : 86%, 95% ee
ADH-R9 : 90%, 97% ee
ADH-R10 : 88%, 92% ee

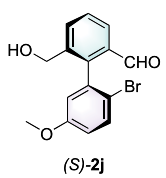

(S)-**2j**

ADH-R2 : 81%, 56% ee
ADH-R4 : 72%, 44% ee

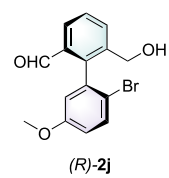

(R)-**2j**

ADH-R1 : 95%, 99% ee
ADH-R9 : 45%, 64% ee
ADH-R10 : 36%, 58% ee

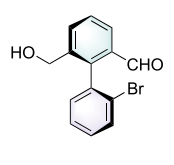

(S)-**2k**

ADH-R7 : 76%, 55% ee
ADH-R9 : 87%, 66% ee
ADH-R10 : 75%, 47% ee

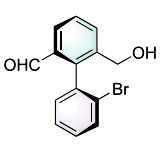

(R)-**2k**

ADH-R1 : 20%, 74% ee
ADH-R2 : 12%, 93% ee

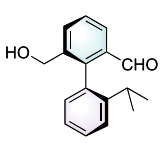

(S)-**2l**

ADH-R1 : 90%, 10% ee
ADH-R2 : 70%, > 99% ee
ADH-R4 : > 99%, > 99% ee

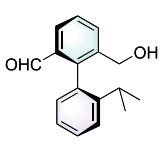

(R)-**2l**

ADH-R7 : 86%, 85% ee
ADH-R9 : 89%, 87% ee
ADH-R10 : 85%, 81% ee

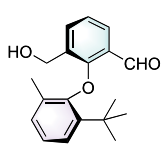

(S)-**2m**

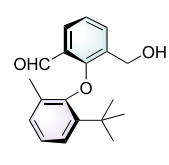

(R)-**2m**

ADH-R7 : 37%, > 99% ee
ADH-R9 : 60%, > 99% ee
ADH-R10 : 35%, > 99% ee

[a]Reaction conditions: **1a** (10 mM), $NADP^+$ (1 mM), glucose (20 mM), GDH (2.5 mg mL^{-1}), ADHs (0.1 g mL^{-1} of whole cell with 6 units mL^{-1} of DNaseI and 1 mg mL^{-1} of lysozyme), DMSO (5% v/v) in NaPi buffer (pH 7.4, 50 mM), at 30 °C, 3−24 h, 800 rpm. Total volume: 1 mL. *3b (5% by ADH-R2), **3c** (3% by ADH-R1), **3i** (3% by ADH-R7), **3k** (16% by ADH-R1 and 53% by ADH-R2), **3l** (2% by ADH-R1) were formed at the sampling time, and the diol products were not found for the rest of the substrates.

phenyl (**1e**), methyl (**1h**), vinyl (**1i**), halogen (**1k**), or alkyl (**1l**) substituents on phenyl rings of the dialdehydes react well to furnish the desired biaryl monoaldehyde atropisomers at up to 99% yields with access to both (*R*)- and (*S*)-configured products in up to 99% ee. (*R*)-**2j** with two substitutions has been obtained in excellent ee, but only moderate to good yields and ee have been obtained for (*S*)-**2j**. The diaryl ether product (*R*)-**2m** was obtained in good yields and excellent ee (up to 99%), but no enzyme showed (*S*)-selectivity for this substrate. ADH-R1, -R2, and -R4 catalyzed the formation of (*S*)-configured products for the substrates **1a**, **1b**, **1c**, **1g**, **1h**, **1i**, and **1l**. Correspondingly, (*R*)-monoaldehydes can be obtained for the same range of substrates catalyzed by ADH-R7, ADH-R9, and ADH-R10. These substrates have relatively large or hydrophobic motifs at the phenyl ring and may have situated in the active sites of the enzymes in similar poses. However, when the size of the substituent increases to the anthracyl group, ADH-R1, -R9, and -R10 all catalyze the formation of (*S*)-**2f**, thereby indicating different binding modes compared with the model substrate. The selectivity for ADH-R7, -R9, and -R10

https://doi.org/10.1021/jacsau.3c00814
JACS Au 2024, 4, 411−418

Scheme 3. Semipreparative Scale Reactions and Synthetic Transformations of Atropisomeric Biaryls

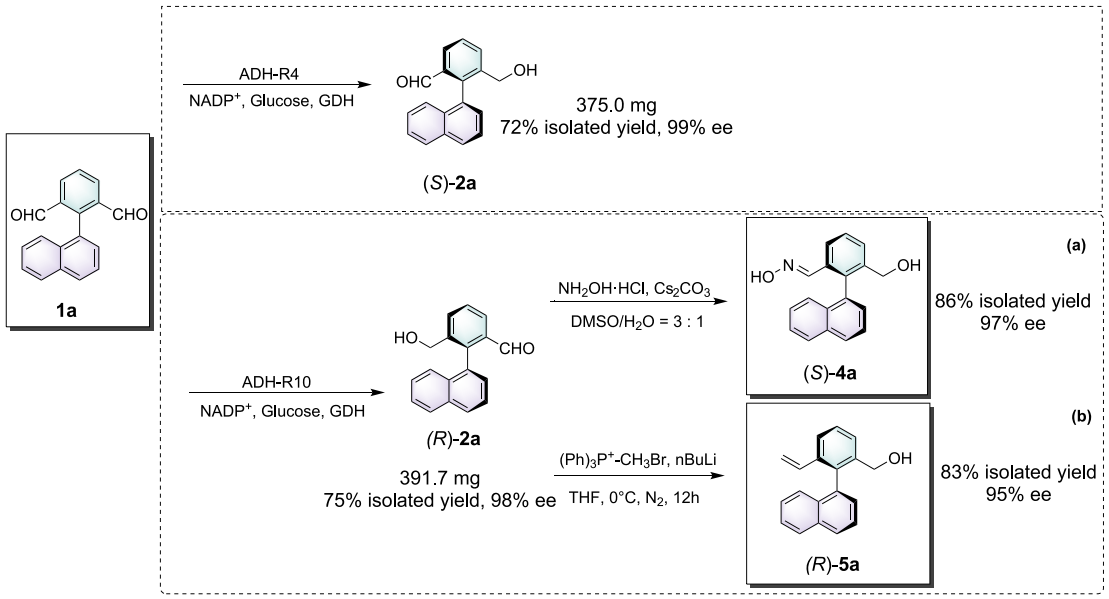

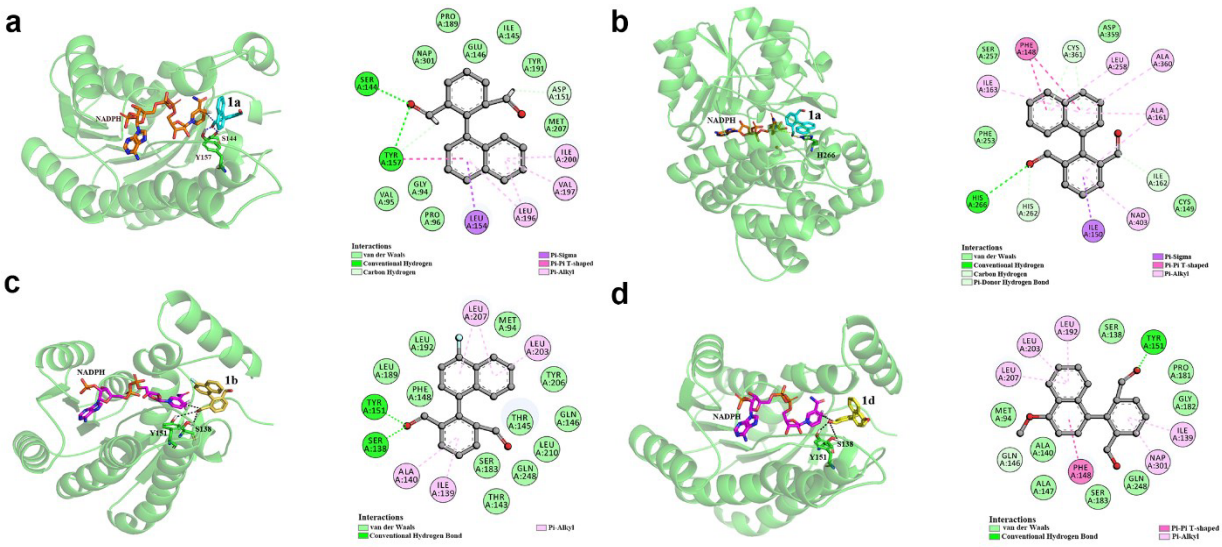

Figure 1. Investigations into the origin of atroposelectivity. (a) Docking model of **1a** at ADH-R4. (b) Docking model of **1a** at ADH-R10. (c) Docking model of **1b** at ADH-R1. (d) Docking model of **1d** at ADH-R1.

are reversed utilizing **1k** as the substrate, and this is possibly due to change in the Cahn–Ingold–Prelog rule for **2k** compared with **2a**. This is not the case for **2k** and **2h,** which display reversed selectivity possibly due to different interactions between the substrates and the enzymes (Figure S3). Overall, there is no definitive correlation between the type of substituent and the selectivity. Further mechanisms of the enzymatic recognition of substrates have been analyzed to provide explanations at molecular levels.

Subsequently, we demonstrated synthetic applications of the ADH-catalyzed atroposelective desymmetrization of biaryl dialdehydes by performing semipreparative scale reaction of **1a** with ADH-R10 to afford (*R*)-**2a** and ADH-R4 to afford (*S*)-**2a** (Scheme 3). The isolated products were obtained, respectively in 375.0 and 391.7 mg amounts with almost perfect ee (98–99%) and good isolated yields (72–75%). Further derivatization of the atropisomeric (*R*)-**2a** is illustrated in Scheme 3. Condensation with hydroxylamine hydrochloride produced **4a** in 86% isolated yield and 97% ee (Scheme 3a). (*R*)-**2a** could also undergo a Wittig reaction to afford **5a** in 83% isolated yield and 95% ee (Scheme 3b).

To gain further insights into the interactions between the substrates and key binding residues of the enzymes and the mechanisms underlying atroposelectivity, docking of **1a** to binding sites of ADH-R4 and ADH-R10 were performed utilizing Autodock 4.2, respectively.[57] ADH-R4 and ADH-R10 afforded either (*S*)-**2a** or (*R*)-**2a** with >99% ee, respectively. ADH-R4 is a SDR from *Oenococcus alcoholitolerans* (KGO31568.1), and ADH-R10 is an MDR from *Pseudomonas meliae* (WP_044345496.1). We predicted the structures using AlphaFold2[58] and identified the positions of the cofactor of ADH-R4 and ADH-R10 with reference to the previously

https://doi.org/10.1021/jacsau.3c00814
JACS Au 2024, 4, 411–418

reported crystal structures (PDB ID: 4RF2 and 3OX4). Subsequently, the interactions between the substrate and enzymes were analyzed (Figure 1a,b). The residues S144 and Y157 from ADH-R4 form hydrogen bonds with the substrate, which is the main driving force for **1a** to situate at a position where the pro-S hydroxyl group points to the catalytic hydride transfer site of the cofactor NADPH. In addition, interactions to the naphthyl ring by surrounding residues can also be observed, which may also contribute to the binding pose of **1a**. Similarly, hydrogen bonds between residue H266 and the hydroxyl group at **1a** are the major contributing factor for the formation of (*R*)-**2a**. Therefore, **1a** is situated in different positions at different binding pockets of ADHs, which leads to reversed atroposelectivity.

Furthermore, pro-atropisomeric **1b** and **1d** were converted to (*S*)-**2b** and (*R*)-**2d** by ADH-R1, respectively (Figure 1c,d). Both substrates were docked into ADH-R1 from *Burkholderia gladioli* (WP_013688875.1, structure predicted by AlphaFold2). The residues Y151 and S138 at ADH-R1 form hydrogen bonds with the carbonyl group at **1b**, whereas only Y151 forms hydrogen bonds with **1d**. This difference is possibly the origin of the lower atroposelectivity for ADH-R1 toward **1d** than **1b** and it correlates well with the experimental results. In addition, the naphthyl rings at **1b** and **1d** are positioned differently. π-Alkyl interactions are observed between residues L203 and L207 and the naphthyl ring of **1b**, whereas additional $\pi-\pi$ or π-alkyl interactions are formed between residues L192 and F148 and the naphthyl ring at **1d** because of a different binding pose of **1d** caused by steric hindrance of the methoxy substitutions at **1d**. Therefore, with only the replacement of fluoro- to methoxy-substitution at the naphthyl rings of the substrates, the configuration of the products is reversed. In summary, the recognition of pro-atropisomeric substrates and origin of atroposelectivity of ADHs are distinct from the center-chiral substrates where the dihedral angle for the hydride transfer to the carbonyl groups on the substrates is the major contributing factor to the configuration of the products.[59,60]

CONCLUSIONS

In summary, we have developed the highly efficient asymmetric synthesis of axially chiral biaryls and diaryl ethers by ADH-catalyzed desymmetrization. Several ADHs were identified and characterized to catalyze the formation of a range of atropisomeric monoaldehydes in moderate to excellent ee and yields with both (*R*)- and (*S*)-configuration. The reactions are easy to scale up with good to high isolated yields and can be further derivatized to afford novel products. The current methodologies greatly expand the scope of enzymatic atroposelective reactions of biaryls and diaryl ethers. Future work may include engineering of the enzymes with the purpose of improving the selectivity and activity for the stereodivergent synthesis of axially chiral products to meet application requirements.

ASSOCIATED CONTENT

Supporting Information

The Supporting Information is available free of charge at https://pubs.acs.org/doi/10.1021/jacsau.3c00814.

General information, preparation of alcohol dehydrogenases, procedures for molecular docking simulations and alcohol dehydrogenases-catalyzed desymmetrization of biaryl dialdehydes, supplementary figures, synthesis of substrates, HPLC, and ^{1}H and ^{13}C NMR spectra (PDF)

AUTHOR INFORMATION

Corresponding Authors

Bo Yuan − *Tianjin Institute of Industrial Biotechnology, Chinese Academy of Sciences, Tianjin 300308, China; Key Laboratory of Engineering Biology for Low-Carbon Manufacturing, Chinese Academy of Sciences, Tianjin 300308, China;* orcid.org/0000-0001-5311-0738; Email: yuanb@tib.cas.cn

Zhoutong Sun − *Tianjin Institute of Industrial Biotechnology, Chinese Academy of Sciences, Tianjin 300308, China; Key Laboratory of Engineering Biology for Low-Carbon Manufacturing, Chinese Academy of Sciences, Tianjin 300308, China;* orcid.org/0000-0002-9923-0951; Email: sunzht@tib.cas.cn

Authors

Mengjing Ye − *College of Biotechnology, Tianjin University of Science and Technology, Tianjin 300457, China; Tianjin Institute of Industrial Biotechnology, Chinese Academy of Sciences, Tianjin 300308, China*

Congcong Li − *Tianjin Institute of Industrial Biotechnology, Chinese Academy of Sciences, Tianjin 300308, China; Key Laboratory of Engineering Biology for Low-Carbon Manufacturing, Chinese Academy of Sciences, Tianjin 300308, China*

Dongguang Xiao − *College of Biotechnology, Tianjin University of Science and Technology, Tianjin 300457, China*

Ge Qu − *Tianjin Institute of Industrial Biotechnology, Chinese Academy of Sciences, Tianjin 300308, China; Key Laboratory of Engineering Biology for Low-Carbon Manufacturing, Chinese Academy of Sciences, Tianjin 300308, China;* orcid.org/0000-0002-0711-169X

Complete contact information is available at: https://pubs.acs.org/10.1021/jacsau.3c00814

Author Contributions

#These authors contributed equally. CRediT: **Mengjing Ye** data curation, validation; **Congcong Li** data curation, software; **Dongguang Xiao** conceptualization, supervision; **Ge Qu** conceptualization, supervision; **Bo Yuan** conceptualization, supervision, writing-original draft, writing-review & editing; **Zhoutong Sun** supervision.

Notes

The authors declare no competing financial interest.

ACKNOWLEDGMENTS

This work was supported by the National Natural Science Foundation of China (No. 32171462), the National Key Research and Development Program of China (No. 2019YFA0905100), Tianjin Synthetic Biotechnology Innovation Capacity Improvement Project (No. TSBICIP-CXRC-040), and the Natural Science Foundation Applying System of Tianjin (No. 21JCJQJC00110).

REFERENCES

(1) Christie, G. H.; Kenner, J. The molecular configurations of polynuclear aromatic compounds. Part I. The resolution of γ-6 : 6′-

dinitro- and 4 : 6 : 4′ : 6′-tetranitro-diphenic acids into optically active components. *J. Chem. Soc. Trans.* **1922**, *121*, 614−620.
(2) Bringmann, G.; Gulder, T.; Gulder, T. A. M.; Breuning, M. Atroposelective total synthesis of axially chiral biaryl natural products. *Chem. Rev.* **2011**, *111*, 563−639.
(3) Kozlowski, M. C.; Morgan, B. J.; Linton, E. C. Total synthesis of chiral biaryl natural products by asymmetric biaryl coupling. *Chem. Soc. Rev.* **2009**, *38*, 3193−3207.
(4) Reisberg, S. H.; Gao, Y.; Walker, A. S.; Helfrich, E. J. N.; Clardy, J.; Baran, P. S. Total synthesis reveals atypical atropisomerism in a small-molecule natural product, tryptorubin A. *Science* **2020**, *367*, 458−463.
(5) Aldemir, H.; Richarz, R.; Gulder, T. A. M. The biocatalytic repertoire of natural biaryl formation. *Angew. Chem., Int. Ed.* **2014**, *53*, 8286−8293.
(6) Pu, L. Enantioselective fluorescent sensors: a tale of binol. *Acc. Chem. Res.* **2012**, *45*, 150−163.
(7) Zhang, D. W.; Li, M.; Chen, C. F. Recent advances in circularly polarized electroluminescence based on organic light-emitting diodes. *Chem. Soc. Rev.* **2020**, *49*, 1331−1343.
(8) Zhang, Y.; Calupitan, J. P.; Rojas, T.; Tumbleson, R.; Erbland, G.; Kammerer, C.; Ajayi, T. M.; Wang, S.; Curtiss, L. A.; Ngo, A. T.; Ulloa, S. E.; Rapenne, G.; Hla, S. W. A chiral molecular propeller designed for unidirectional rotations on a surface. *Nat. Commun.* **2019**, *10*, 3742.
(9) Clayden, J.; Moran, W. J.; Edwards, P. J.; LaPlante, S. R. The challenge of atropisomerism in drug discovery. *Angew. Chem., Int. Ed.* **2009**, *48*, 6398−6401.
(10) LaPlante, S. R.; Fader, L. D.; Fandrick, K. R.; Fandrick, D. R.; Hucke, O.; Kemper, R.; Miller, S. P. F.; Edwards, P. J. Assessing atropisomer axial chirality in drug discovery and development. *J. Med. Chem.* **2011**, *54*, 7005−7022.
(11) Glunz, P. W. Recent encounters with atropisomerism in drug discovery. *Bioorg. Med. Chem. Lett.* **2018**, *28*, 53−60.
(12) Wencel-Delord, J.; Panossian, A.; Leroux, F. R.; Colobert, F. Recent advances and new concepts for the synthesis of axially stereoenriched biaryls. *Chem. Soc. Rev.* **2015**, *44*, 3418−3430.
(13) Cheng, J. K.; Xiang, S. H.; Li, S.; Ye, L.; Tan, B. Recent advances in catalytic asymmetric construction of atropisomers. *Chem. Rev.* **2021**, *121*, 4805−4902.
(14) Kumarasamy, E.; Raghunathan, R.; Sibi, M. P.; Sivaguru, J. Nonbiaryl and heterobiaryl atropisomers: molecular templates with promise for atropselective chemical transformations. *Chem. Rev.* **2015**, *115*, 11239−11300.
(15) Mei, G. J.; Koay, W. L.; Guan, C. Y.; Lu, Y. Atropisomers beyond the C−C axial chirality: advances in catalytic asymmetric synthesis. *Chem.* **2022**, *8*, 1855−1893.
(16) Bai, X. F.; Cui, Y. M.; Cao, J.; Xu, L. W. Atropisomers with axial and point chirality: synthesis and applications. *Acc. Chem. Res.* **2022**, *55*, 2545−2561.
(17) Carmona, J. A.; Rodriguez-Franco, C.; Fernandez, R.; Hornillos, V.; Lassaletta, J. M. Atroposelective transformation of axially chiral (hetero)biaryls. From desymmetrization to modern resolution strategies. *Chem. Soc. Rev.* **2021**, *50*, 2968−2983.
(18) Di Iorio, N.; Crotti, S.; Bencivenni, G. Organocatalytic desymmetrization reactions for the synthesis of axially chiral compounds. *Chem. Rec.* **2019**, *19*, 2095−2104.
(19) Lassaletta, J. M. *Atropisomerism and Axial Chirality*; World Scientific Publishing Co Pte Ltd: Singapore, 2019.
(20) Xiang, S. H.; Tan, B. Advances in asymmetric organocatalysis over the last 10 years. *Nat. Commun.* **2020**, *11*, 3786.
(21) Wang, Y. B.; Tan, B. Construction of axially chiral compounds via asymmetric organocatalysis. *Acc. Chem. Res.* **2018**, *51*, 534−547.
(22) Zhao, C.; Guo, D.; Munkerup, K.; Huang, K. W.; Li, F.; Wang, J. Enantioselective [3 + 3] atroposelective annulation catalyzed by N-heterocyclic carbenes. *Nat. Commun.* **2018**, *9*, 611.
(23) Xu, K.; Li, W.; Zhu, S.; Zhu, T. Atroposelective arene formation by carbene-catalyzed formal [4 + 2] cycloaddition. *Angew. Chem., Int. Ed.* **2019**, *58*, 17625−17630.
(24) Yang, X.; Wei, L.; Wu, Y.; Zhou, L.; Zhang, X.; Chi, Y. R. Atroposelective access to 1,3-oxazepine-containing bridged biaryls via carbene-catalyzed desymmetrization of imines. *Angew. Chem., Int. Ed.* **2023**, *62*, No. e202211977.
(25) Lv, Y.; Luo, G.; Liu, Q.; Jin, Z.; Zhang, X.; Chi, Y. R. Catalytic atroposelective synthesis of axially chiral benzonitriles via chirality control during bond dissociation and CN group formation. *Nat. Commun.* **2022**, *13*, 36.
(26) Yang, G.; Guo, D.; Meng, D.; Wang, J. NHC-catalyzed atropoenantioselective synthesis of axially chiral biaryl amino alcohols via a cooperative strategy. *Nat. Commun.* **2019**, *10*, 3062.
(27) Song, R.; Xie, Y.; Jin, Z.; Chi, Y. R. Carbene-catalyzed asymmetric construction of atropisomers. *Angew. Chem., Int. Ed.* **2021**, *60*, 26026−26037.
(28) Bao, H.; Chen, Y.; Yang, X. Catalytic asymmetric synthesis of axially chiral diaryl ethers through enantioselective desymmetrization. *Angew. Chem., Int. Ed.* **2023**, *62*, No. e202300481.
(29) Dai, L.; Liu, Y.; Xu, Q.; Wang, M.; Zhu, Q.; Yu, P.; Zhong, G.; Zeng, X. A dynamic kinetic resolution approach to axially chiral diaryl ethers by catalytic atroposelective transfer hydrogenation. *Angew. Chem., Int. Ed.* **2023**, *62*, No. e202216534.
(30) Vaidya, S. D.; Toenjes, S. T.; Yamamoto, N.; Maddox, S. M.; Gustafson, J. L. Catalytic atroposelective synthesis of N-aryl quinoid compounds. *J. Am. Chem. Soc.* **2020**, *142*, 2198−2203.
(31) Bai, H. Y.; Tan, F.X.; Liu, T.Q.; Zhu, G.D.; Tian, J.M.; Ding, T.M.; Chen, Z.M.; Zhang, S.Y. Highly atroposelective synthesis of nonbiaryl naphthalene-1,2-diamine N-C atropisomers through direct enantioselective C-H amination. *Nat. Commun.* **2019**, *10*, 3063.
(32) Chen, K. W.; Chen, Z. H.; Yang, S.; Wu, S. F.; Zhang, Y. C.; Shi, F. Organocatalytic atroposelective synthesis of N−N axially chiral indoles and pyrroles by de novo ring formation. *Angew. Chem., Int. Ed.* **2022**, *61*, No. e2021168.
(33) Mori, K.; Ichikawa, Y.; Kobayashi, M.; Shibata, Y.; Yamanaka, M.; Akiyama, T. Enantioselective synthesis of multisubstituted biaryl skeleton by chiral phosphoric acid catalyzed desymmetrization/kinetic resolution sequence. *J. Am. Chem. Soc.* **2013**, *135*, 3964−3970.
(34) Zheng, S. C.; Wu, S.; Zhou, Q.; Chung, L. W.; Ye, L.; Tan, B. Organocatalytic atroposelective synthesis of axially chiral styrenes. *Nat. Commun.* **2017**, *8*, 15238.
(35) Munday, E. S.; Grove, M. A.; Feoktistova, T.; Brueckner, A. C.; Walden, D. M.; Young, C. M.; Slawin, A. M. Z.; Campbell, A. D.; Cheong, P. H.; Smith, A. D. Isothiourea-catalyzed atropselective acylation of biaryl phenols via sequential desymmetrization /Kinetic Resolution. *Angew. Chem., Int. Ed.* **2020**, *59*, 7897−7905.
(36) Yu, C.; Huang, H.; Li, X.; Zhang, Y.; Wang, W. Dynamic kinetic resolution of biaryl lactones via a chiral bifunctional amine thiourea-catalyzed highly atropo-enantioselective transesterification. *J. Am. Chem. Soc.* **2016**, *138*, 6956−9.
(37) Gustafson, J. L.; Lim, D.; Miller, S. J. Dynamic kinetic resolution of biaryl atropisomers via peptide-catalyzed asymmetric bromination. *Science* **2010**, *328*, 1251−1255.
(38) Cen, S.; Huang, N.; Lian, D.; Shen, A.; Zhao, M. X.; Zhang, Z. Conformational enantiodiscrimination for asymmetric construction of atropisomers. *Nat. Commun.* **2022**, *13*, 4735.
(39) Luo, J.; Zhang, T.; Wang, L.; Liao, G.; Yao, Q. J.; Wu, Y. J.; Zhan, B. B.; Lan, Y.; Lin, X. F.; Shi, B. F. Enantioselective synthesis of biaryl atropisomers by Pd-catalyzed C-H olefination using chiral spiro phosphoric acid ligands. *Angew. Chem., Int. Ed.* **2019**, *58*, 6708−6712.
(40) Yao, W.; Lu, C. J.; Zhan, L. W.; Wu, Y.; Feng, J.; Liu, R. R. Enantioselective synthesis of N-N atropisomers by palladium-catalyzed C-H functionalization of pyrroles. *Angew. Chem., Int. Ed.* **2023**, *62*, No. e202218871.
(41) Gu, X. W.; Sun, Y. L.; Xie, J. L.; Wang, X. B.; Xu, Z.; Yin, G. W.; Li, L.; Yang, K. F.; Xu, L. W. Stereospecific Si-C coupling and remote control of axial chirality by enantioselective palladium-catalyzed hydrosilylation of maleimides. *Nat. Commun.* **2020**, *11*, 2904.
(42) Zhang, J.; Wang, J. Atropoenantioselective redox-neutral amination of biaryl compounds through borrowing hydrogen and dynamic kinetic resolution. *Angew. Chem., Int. Ed.* **2018**, *57*, 465−469.

https://doi.org/10.1021/jacsau.3c00814
JACS Au 2024, 4, 411−418

(43) Feng, J.; Bi, X.; Xue, X.; Li, N.; Shi, L.; Gu, Z. Catalytic asymmetric C-Si bond activation via torsional strain-promoted Rh-catalyzed aryl-Narasaka acylation. *Nat. Commun.* **2020**, *11*, 4449.
(44) Zhu, M.; Jiang, H. J.; Sharanov, I.; Irran, E.; Oestreich, M. Atroposelective silylation of 1,1′-biaryl-2,6-diols by a chiral counter-anion directed desymmetrization enhanced by a subsequent kinetic resolution. *Angew. Chem., Int. Ed.* **2023**, *62*, No. e202304475.
(45) Wu, Y.; Li, M.; Sun, J.; Zheng, G.; Zhang, Q. Synthesis of axially chiral aldehydes by N-Heterocyclic-Carbene-Catalyzed desymmetrization followed by kinetic resolution. *Angew. Chem., Int. Ed.* **2022**, *61*, No. e202117340.
(46) Watts, O. F. B.; Berreur, J.; Collins, B. S. L.; Clayden, J. Biocatalytic enantioselective synthesis of atropisomers. *Acc. Chem. Res.* **2022**, *55*, 3362−3375.
(47) Skrobo, B.; Rolfes, J. D.; Deska, J. Enzymatic approaches for the preparation of optically active non-centrochiral compounds. *Tetrahedron* **2016**, *72*, 1257−1275.
(48) Obermaier, S.; Thiele, W.; Furtges, L.; Muller, M. Enantioselective phenol coupling by laccases in the biosynthesis of fungal dimeric naphthopyrones. *Angew. Chem., Int. Ed.* **2019**, *58*, 9125−9128.
(49) Guo, H.; Sun, N.; Guo, J.; Zhou, T. P.; Tang, L.; Zhang, W.; Deng, Y.; Liao, R. Z.; Wu, Y.; Wu, G.; Zhong, F. Expanding the promiscuity of a copper-dependent oxidase for enantioselective cross-coupling of indoles. *Angew. Chem., Int. Ed.* **2023**, *62*, No. e202219034.
(50) Zetzsche, L. E.; Yazarians, J. A.; Chakrabarty, S.; Hinze, M. E.; Murray, L. A. M.; Lukowski, A. L.; Joyce, L. A.; Narayan, A. R. H. Biocatalytic oxidative cross-coupling reactions for biaryl bond formation. *Nature* **2022**, *603*, 79−85.
(51) Girol, C. G.; Fisch, K. M.; Heinekamp, T.; Guenther, S.; Huettel, W.; Piel, J.; Brakhage, A. A.; Mueller, M. Regio-and stereoselective oxidative phenol coupling in *Aspergillus niger*. *Angew. Chem., Int. Ed.* **2012**, *51*, 9788−9791.
(52) Mazzaferro, L. S.; Huettel, W.; Fries, A.; Mueller, M. Cytochrome P450-catalyzed regio- and stereoselective phenol coupling of fungal natural products. *J. Am. Chem. Soc.* **2015**, *137*, 12289−12295.
(53) Huang, W.; Huang, S.; Sun, Z.; Zhang, W.; Zeng, Z.; Yuan, B. Chemoenzymatic synthesis of sterically hindered biaryls by Suzuki coupling and vanadium chloroperoxidase catalyzed halogenations. *ChemBioChem.* **2023**, *24*, No. e202200610.
(54) Yuan, B.; Page, A.; Worrall, C. P.; Escalettes, F.; Willies, S. C.; McDouall, J. J. W.; Turner, N. J.; Clayden, J. Biocatalytic desymmetrization of an atropisomer with both an enantioselective oxidase and ketoreductases. *Angew. Chem., Int. Ed.* **2010**, *49*, 7010−7013.
(55) Staniland, S.; Yuan, B.; Gimenez-Agullo, N.; Marcelli, T.; Willies, S. C.; Grainger, D. M.; Turner, N. J.; Clayden, J. Enzymatic desymmetrising redox reactions for the asymmetric synthesis of biaryl atropisomers. *Chem.—Eur. J.* **2014**, *20*, 13084−13088.
(56) Staniland, S.; Adams, R. W.; McDouall, J. J. W.; Maffucci, I.; Contini, A.; Grainger, D. M.; Turner, N. J.; Clayden, J. Biocatalytic dynamic kinetic resolution for the synthesis of atropisomeric biaryl N-oxide Lewis base catalysts. *Angew. Chem., Int. Ed.* **2016**, *55*, 10755−10759.
(57) Morris, G. M.; Huey, R.; Lindstrom, W.; Sanner, M. F.; Belew, R. K.; Goodsell, D. S.; Olson, A. J. AutoDock4 and AutoDockTools4: automated docking with selective receptor flexibility. *J. Comput. Chem.* **2009**, *30*, 2785−2791.
(58) Jumper, J.; Evans, R.; Pritzel, A.; Green, T.; Figurnov, M.; Ronneberger, O.; Tunyasuvunakool, K.; Bates, R.; Zidek, A.; Potapenko, A.; Bridgland, A.; Meyer, C.; Kohl, S. A. A.; Ballard, A. J.; Cowie, A.; Romera-Paredes, B.; Nikolov, S.; Jain, R.; Adler, J.; Back, T.; Petersen, S.; Reiman, D.; Clancy, E.; Zielinski, M.; Steinegger, M.; Pacholska, M.; Berghammer, T.; Bodenstein, S.; Silver, D.; Vinyals, O.; Senior, A. W.; Kavukcuoglu, K.; Kohli, P.; Hassabis, D. Highly accurate protein structure prediction with AlphaFold. *Nature* **2021**, *596*, 583−589. Jumper, J.; Evans, R.; Pritzel, A.; Green, T.; Figurnov, M.; Ronneberger, O.; Tunyasuvunakool, K.; Bates, R.; Zidek, A.; Potapenko, A.; Bridgland, A.; Meyer, C.; Kohl, S. A. A.; Ballard, A. J.; Cowie, A.; Romera-Paredes, B.; Nikolov, S.; Jain, R.; Adler, J.; Back, T.; Petersen, S.; Reiman, D.; Clancy, E.; Zielinski, M.; Steinegger, M.; Pacholska, M.; Berghammer, T.; Bodenstein, S.; Silver, D.; Vinyals, O.; Senior, A. W.; Kavukcuoglu, K.; Kohli, P.; Hassabis, D. Highly accurate protein structure prediction with AlphaFold. *Nature* **2021**, *596*, 583−589.
(59) Qu, G.; Bi, Y.; Liu, B.; Li, J.; Han, X.; Liu, W.; Jiang, Y.; Qin, Z.; Sun, Z. Unlocking the stereoselectivity and substrate acceptance of enzymes: proline-induced loop engineering test. *Angew. Chem., Int. Ed.* **2022**, *61*, No. e202110793.
(60) Jiang, Y.; Qu, G.; Sheng, X.; Tong, F.; Sun, Z. Unraveling the mechanism of enantio-controlling switches of an alcohol dehydrogenase toward sterically small ketone. *Catal. Sci. Technol.* **2022**, *12*, 1777−1787.

https://doi.org/10.1021/jacsau.3c00814
JACS Au 2024, 4, 411−418